CHIN. PHYS. LETT. Vol. 26, No. 11 (2009) 114204

Polarization-Independent Directional Beaming of Light by a Subwavelength Metal Slit

ZHANG Xiang(张翔)**, LI Cheng-Fang(李承芳)

Department of Physics, Wuhan University, Wuhan 430072

(Received 1 April 2009)

We present the directional beaming effect of light at the terahertz frequency by using a subwavelength slit in the metal film. The metal is dressed with anisotropic dielectric so that both the transverse electric (TE) and transverse magnetic (TM) polarized waves can be well guided on the metal surface and reach the phase matching. By using a periodical array of dielectric ridges and grooves around the slit, the guided waves can be scattered out of the slit and interfere with the transmitted light directly through the slit. The results performed by finite-difference at time-domain computations indicate that the directional beaming of light can be obtained simultaneously for both the TE and TM polarized waves after optimizing the geometric parameters. The structure may find great applications in polarization-independent optical devices such as couplers, connectors, beam collimator, and etc.

PACS: 42. 79. Ag, 42. 68. Mj

Light usually spreads out in all directions when passing through a slit with subwavelength width, due to the diffraction effect. Recently, it has been reported that light can be directionally beamed with subwavelength metal slits flanked by periodical grooves or by dielectric gratings.[1−3] The underlying physics and potential applications concerning this phenomenon have attracted much attention.[4−6] Basically, the beaming effect stems from the resonance of wave emission on metal surfaces,[4,5] of which the surface plasmon is convinced to play a major role. Note that surface plasmons must be excited by transverse magnetic (TM) polarized waves.[7] Relevant research[8−10] on transverse electric (TE) polarized waves has also been performed to find analogous applications without the involvement of surface plasmons. In many previous works, the considered wavelength lies mainly in the infrared or visible range since surface plasmons at shorter wavelength could be more tightly confined on metal surfaces.[11] As an interesting wave range, the terahertz (THz) waves, which bridge the gap between microwaves and visible range, also find important applications in many fields.[12−15] Naively, the beaming effect seems applying to THz waves according to the scaling law, however it is not obvious because metals at THz frequencies hold a huge conductivity and show a weak wave confinement.

In this work, we study the directional beaming of light at the THz frequency by using a subwavelength slit for both the TE and TM polarizations. Although both polarized waves in low frequencies cannot be well confined on bare metal surfaces, the metal dressed with a thin dielectric film could realize a good confinement of both waves.[13] Notably, the anisotropic dielectric is employed such that the two polarized waves could be modulated separately to reach a phase matching. By using the finite-difference at time-domain (FDTD) method,[16] we evidence that the TE and TM waves transmitted through the slit can be directionally beamed at the same time. The result extends the applications of directional beaming effect to polarization-independent devices[17] and to THz wave range.

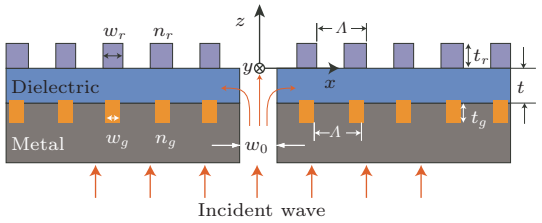


Fig. 1. Sketch of the slit structure for directional beaming of light. The slit has a width of w_0; the thickness of the metal is 0.48λ; t and ε_d denote the thickness and dielectric constant of the dielectric film; the periods of ridges and grooves both are Λ; t_r and t_g represent the height of the ridges and the depth of the grooves while their width are w_r and w_g; n_r and n_g are refractive indices of the ridges and grooves.

The structure proposed to realize directional beaming of light is depicted in Fig. 1. The metal film with a thickness of 0.48λ is perforated by a slit with a width of w_0, where λ represents the wavelength. The frequency of the incident wave is fixed at 1 THz ($\lambda = 300\,\mu$m). The dielectric constant of the metal is taken from the Drude model: $\varepsilon_m = \varepsilon_\infty - \omega_p^2/[\omega(\omega + j\gamma)]$, with $\varepsilon_\infty = 1$, $\omega_p = 1.37 \times 10^4$ THz, and $\gamma = 40.7$ THz, appropriate for gold,[18] where ω stands for the frequency of the incident wave. A dielectric film with a thickness of t is deposited on the metal, ε_d ($= n^2$, n is the refractive index) represents the dielectric constant of the dielectric. The slit is flanked by periodic arrays of ridges on the dielectric and grooves in the metal. The periods of the ridges and grooves both

**Email: xzhang@whu.edu.cn

© 2009 Chinese Physical Society and IOP Publishing Ltd

are Λ. The length of the ridges and the depth of the grooves are denoted by t_r and t_g, while their widths are w_r and w_g, respectively; n_r and n_g represent the refractive indices of ridges and grooves. With respect to the metal slit, the TM waves (magnetic field vertical to xz-plane) can always pass smoothly. Nevertheless, TE waves (electric field vertical to xz-plane) are only permitted when the slit width is larger than $\lambda/2$. Thereafter we fix $w_0 = 0.52\lambda$ for the sake of enough transmission.

When a plane wave impinges on the slit from the bottom, the scattered light at the output will be partly converted into guided modes in the metal-dielectric waveguide formed with a dielectric-dressed metal surface as shown in the inset of Fig. 2(a). Let us first consider the guided modes in the metal-dielectric waveguide and the dispersion relation, which can be easily obtained according to Maxwell's equations and boundary conditions.[19] For the guided mode of lowest order, the dispersion relation can be written as

$$kw = \tan^{-1}\left[\left(\frac{\varepsilon_d}{\varepsilon_0}\right)^p \frac{k_c}{k_d}\right] + \tan^{-1}\left[\left(\frac{\varepsilon_d}{\varepsilon_m}\right)^p \frac{k_m}{k_d}\right], \quad (1)$$

where $\varepsilon_0 = 1$, $k_c = (\beta^2 - \varepsilon_0 k_0^2)^{-1/2}$, $k_m = (\beta^2 - \varepsilon_m k_0^2)^{-1/2}$, and $k_d = (\varepsilon_d k_0^2 - \beta^2)^{-1/2}$ with β being the propagation constant of the guided modes and k_0 the wave vector modulus in air. The equation refers to the TE mode as $p = 0$ and to TM mode as $p = 1$. Due to the orientation of the electric field, the TM mode might be surface plamons on the metal while the TE mode is just a conventional normal mode concentrated in the dielectric layer. The effective index of the guided mode reads as $n_{\text{eff}} = \beta/k_0$. To achieve the phase matching of both polarized modes, we employ anisotropic dielectrics on the metal.[20] The dielectric is assumed to be uniaxial and its optical axis is parallel to the y direction. Thus the dielectric constant can be simplified to $\varepsilon_d = n_e^2$ for the TE mode and to $\varepsilon_d = n_o^2$ for the TM mode, where n_o and n_e are ordinary index and extraordinary index, respectively. The dependence of the effective index on the thickness of anisotropic dielectric film (i.e., the dispersion relation) for TE and TM modes is plotted in Fig. 2(a). The data are obtained by solving Eq. (1) with the Newton iteration method in the complex number field. For isotropic dielectrics ($n_e = n_o$), the dispersion curves for different polarizations will never intersect. However, the intersection of the two curves could happen as anisotropic dielectrics are used. For instance, a value of $\text{Re}(n_{\text{eff}}) = 1.36$ has been achieved for both TE and TM modes at $t = 0.32\lambda$ as $n_e = 1.76$ and $n_o = 1.5$. The condition of $n_e > n_o$ is essential to obtain the intersection.

Figures 2(b)–2(e) show the near-field distributions of E_y for TE waves and H_y for TM waves as the incident waves impinges on a slit with bare metal surfaces and with dielectric film on the metal, respectively. Noticing that there are no grooves and ridges around the slit in this discussion, it is found that no waves can be confined in the vicinity of the bare metal surface for TE waves, as shown in Fig. 2(b). For TM waves as shown in Fig. 2(c), one can also find a weak confinement of waves on the metal surface. If the metal is dressed with a thin dielectric film, comparatively, guided modes will be observed propagating along the metal surface for both TE and TM polarizations, as shown in Figs. 2(d) and 2(e). In the above FDTD calculations, we set $n_e = 1.76$, $n_o = 1.50$, and $t = 0.32\lambda$. The effective indices are equivalent for the TE and TM modes by counting the fringe periods. The results convince the validity of the wave confinement and mode modulation by using anisotropic dielectrics on the metal.

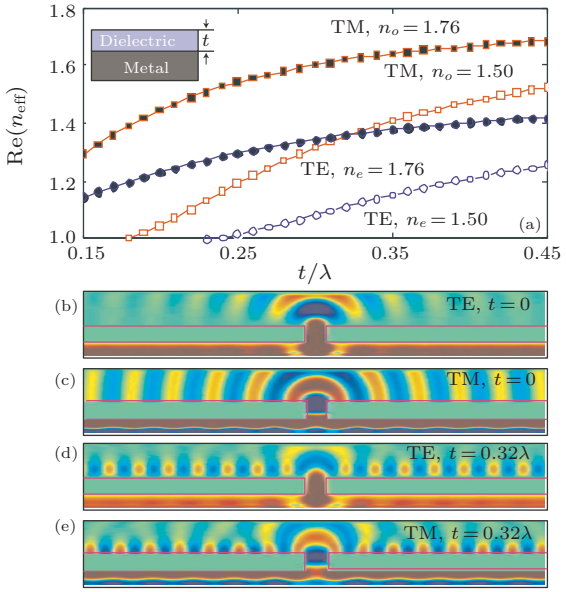


Fig. 2. (a) Dependence of effective index on the thickness of dielectric film for TE and TM modes in the waveguide consisting of metal and anisotropic dielectric (inset). (b) and (c) Distributions of E_y for TE waves and H_y for TM waves when the incident light impinges on a slit with bare metal surface from the bottom. (d) and (e) The same as (b) and (c) but with anisotropic dielectric on the metal with the dielectric thickness $t = 0.32\lambda$. Note that there are no ridges and grooves around the slit.

In order to shape the transmitted light beam from the slit, we also need surface roughness to arouse wave emission from the surface surrounding the slit, which could interfere with the transmitted light directly through the slit. Here we use two types of geometries: the ridges on the dielectric film and grooves in the metal, as shown in Fig. 1. Note that Eq. (1) is no longer valid for the region with ridges, grooves, and the dimensions which will be related to the effective index. The phase matching could be reached by optimizing the ridges and grooves and/or the dielectric layer. As mentioned in the case of metal slit flunked by grooves or by dielectric gratings, the directional beaming of light occurs when the effective wave

length ($\lambda/n_{\rm eff}$) of surfaces waves becomes comparable to the period of the grooves, that is, the condition of in-phase wave emission is satisfied.[4,6] However, the concomitant Bragg reflection will make against the beaming of light because it prevents surface waves from reaching the grooves further from the slit. Actually in our lots of attempts, neither the ridges nor the grooves could single-handedly make an appropriate balance between restricting the Bragg reflection and promoting wave emission for both the TE and TM waves. That is the reason why we use them together in the proposed structures. In Fig. 3, we show how the ridges and grooves together affect the far-field intensity distributions. The field intensity refers to $|E_y|^2$ for TE waves and to $|H_y|^2$ for TM waves. The parameters of the structure (see Fig. 1) are given as $\Lambda = 0.79\lambda$, $t = 0.32\lambda$, $w_r = 0.16\lambda$, $w_g = 0.08\lambda$, $n_g = 1.00$, $n_r = 1.80$, $n_e = 1.60$, $n_o = 1.50$. There are fifteen ridges and grooves on each side of the slit. In the calculation, we firstly obtain the near field distributions by using the FDTD method. The discretization meshes in the FDTD calculations are with the size of $0.008\lambda \times 0.008\lambda$. We have checked that the results are converged by comparing some of the calculations with those performed for other mesh sizes. The far field can be achieved by using the near-to-far-field transformations.[16]

$$\varphi(r) = \int \left[G(r,r') \frac{\partial \varphi(r')}{\partial z} - \varphi(r') \frac{\partial G(r,r')}{\partial z} \right] dx', \quad (2)$$

where $G(\boldsymbol{r},\boldsymbol{r'}) = jH_0^{(1)}\ (k_0|\boldsymbol{r}-\boldsymbol{r'}|)/4$ with $H_0^{(1)}$ being the zero order Hankel function of the first kind, $\boldsymbol{r'} = (x', z')$ and $\boldsymbol{r} = (x, z)$ represent the near-field and far-field coordinates, respectively, $\varphi(r)$ refers to $E_y(\boldsymbol{r})$ for TE waves and to $H_y(\boldsymbol{r})$ for TM waves. The integral in Eq. (2) runs over the x axis at a height of $z' = 0.81\lambda$ on the metal surface. In Figs. 3(a) and 3(b), we fix $t_r = 0.16\lambda$ and vary t_g from 0 to 0.16λ and 0.32λ. From the figures, one can see that as $t_g = 0.32\lambda$, a very narrow peak appears in the normal direction of the metal surface for both TE and TM waves. The divergence angles are 4.2° for TE waves and 3.5° for TM waves. This means both polarized waves are strongly collimated in this situation. Interestingly, one can also see that far-field of TE waves is almost independent of the groove depth t_g, which largely affects the TM waves on the other hand. Because the groove width is much smaller than $\lambda/2$, TE waves cannot exist in the grooves. The scattering of the TE waves by the grooves are very weak. In Figs. 3(c) and 3(d), we fix t_g at 0.32λ and vary t_r from 0 to 0.16λ and 0.32λ. The directional beaming for both the TE and TM waves appears as $t_r = 0.16\lambda$ and 0.32λ. Note that the far field for both the TE and TM waves is insensitive to the variation of ridges higher than 0.16λ. As $t_r = 0$, both of them are scattered in a wide directional range. In brief, the plots in Fig. 3 convince that the very narrow grooves only influence the beaming shape of the TM waves, and the ridges influence those of both TE and TM waves. The results are very useful in the structural design since we can first fix an appropriate value of t_r to realize the directional beaming of the TE waves and then optimize t_g to realize that of TM waves.

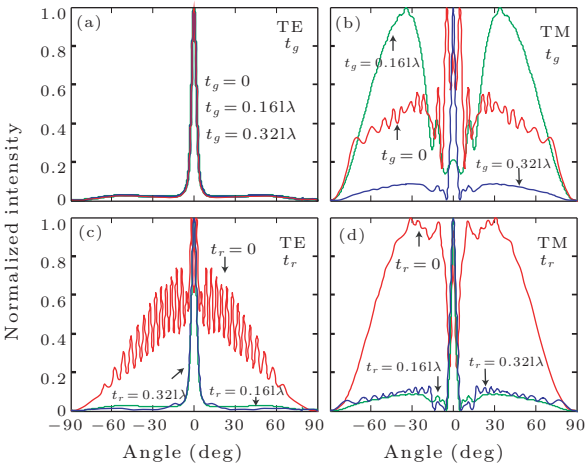


Fig. 3. Far-field profiles of (a) $|E_y|^2$ for TE waves and (b) $|H_y|^2$ for TM waves versus the angle for different groove depth when the structure shown in Fig. 1 is illuminated by a plane wave from the bottom. The red, green, and blue curves refer to $t_g = 0, 0.16\lambda$, and 0.32λ, respectively. Note that the three curves in (a) all merge. (c) and (d) The same as (a) and (b) but for different ridge height. The red, green, and blue curves refer to $t_r = 0$, 0.16λ, and 0.32λ, respectively.

The field distributions of $|E_y|^2$ for TE waves and of $|H_y|^2$ for TM waves as the directional beaming occurs are shown in Figs. 4(a) and 4(b). Here we set $t_r = 0.16\lambda$ and $t_g = 0.32\lambda$. The other parameters are the same as those used in Fig. 3. From Figs. 4(a) and 4(b), one can see that both TE and TM waves are strongly collimated in front of the slit. For TM waves, the noises at large angles [also see the far-field profile in Figs. 3(b) and 3(d)] are mostly due to the diffraction of the slit since they can be removed with a narrower slit (not shown here). The directional beaming of light occurs when the in-phase emission condition satisfies $\mathrm{Re}(n_{\rm eff}^{\sigma})k_0(\Lambda - w_r) + \Delta\varphi^{\sigma} = 2m\pi$, where σ denotes TE or TM polarization, m is an integer, $\Delta\varphi^{\sigma} = k_0 n_{\rm eff}^{\sigma,r}(w_r - w_g) + k_0 n_{\rm eff}^{\sigma,g} w_g$ represents the phase delay when the guided mode passes through the region with ridge and groove, and $n_{\rm eff}^{\sigma}$, $n_{\rm eff}^{\sigma,r}$, $n_{\rm eff}^{\sigma,g}$ stand respectively for the effective index of the region without ridge or groove, with ridge, and with both ridge and groove. The equation implies that the phase delay of guided modes between two adjacent ridges or grooves should be an integer multiple of 2π. If the variation of the effective index for the perturbation is negligible, the equation is simplified to $\mathrm{Re}(n_{\rm eff})k_0\Lambda \approx 2m\pi$ for both TE and TM waves. With the values of n_o and n_e used in Figs. 2(d) and 2(e), we have $\mathrm{Re}(n_{\rm eff}) = 1.36$ for both polarizations,

which means that a period of 0.74λ for the ridges and grooves is required to realize the directional beaming. The predicted value is very close to that of our design ($\Lambda = 0.79\lambda$). Because the effective index of the TM mode will actually increase for the addition of the ridges and decrease for that of grooves, respectively,[10] the in-phase condition could be satisfied for the TM waves after optimize the dimensions of the ridges and grooves. For the TE waves, we have optimized n_e in the implementation to balance the increase of effective index aroused by the ridges, considering that the grooves will almost not affect the phase of TE mode. Figure 4(c) presents the dependence of the divergence angle of the beamed TE and TM waves on the number of ridges and grooves. The divergence angle is obtained by calculating the full width at half maximum of the far-field angle distribution curve (see Fig. 3) as the directional beaming occurs. It is apparent from Fig. 4(c) that the divergence angle for both polarizations decreases with the increased number of ridges and grooves. That should be attributed to the increasing amount of wave emission from the surface around the slit. It should be mentioned that the very similar results could be obtained in the same structure composed of perfect conductors. The influence of finite skin depth of metals on the beaming effect at THz frequency is negligible.

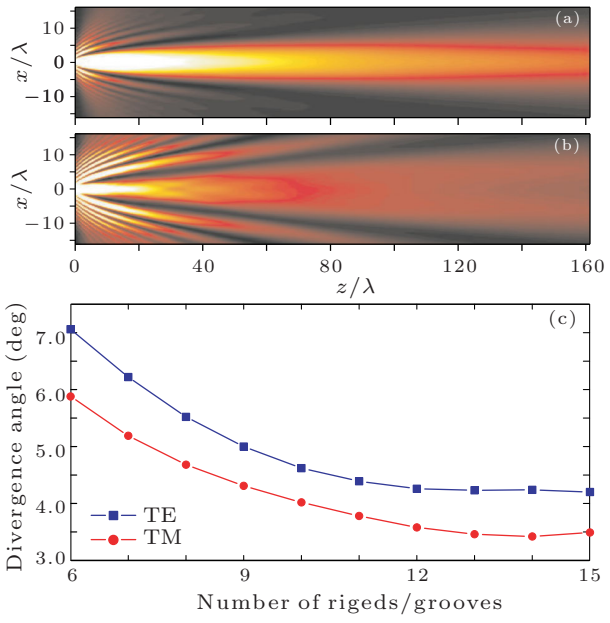


Fig. 4. Distributions of (a) $|E_y|^2$ for TE and (b) $|H_y|^2$ for TM waves in front of the slit as the directional beaming occurs. (c) Divergence angle of TE and TM waves as a function of the number of ridges and grooves.

In conclusion, we have proposed a structure of subwavelength metal slit to realize the directional beaming of light for both the TE and TM polarizations at THz frequency. The metal is dressed with anisotropic dielectric so that the confined TE and TM modes on the metal surface can be modulated separately. The ridges and grooves around the slit could arouse scattered waves that interfere with the directly transmitted light through the slit, resulting in the field redistribution at the slit output. The wave scattering can be tailored by varying the dimensions of the ridges and grooves. After optimization, we observe the directional beaming of both the TE and TM waves at the same time. The very narrow divergence angles of 4.2° and 3.5° are obtained for TE and TM waves, respectively. The structure may find great applications in polarization-independent optical devices such as couplers, connectors, and the beam collimator.

References

[1] Lezec H J, Degiron A, Devaux E, Linke R A, Martín-Moreno L, García-Vidal F J and Ebbesen T W 2002 *Science* **297** 820
[2] Lin D Z, Chang C K, Chen Y C, Yang D L, Lin M W, Yeh J T, Liu J M, Kuan C H, Yeh C S and Lee C K 2006 *Opt. Express* **14** 3503
[3] Li Z B, Tian J G, Zhou W Y, Liu Z B, Zang W P and Zhang C P 2006 *Chin. Phys. Lett.* **23** 1207
[4] Martín-Moreno L, García-Vidal F J, Lezec H J, Degiron A and Ebbesen T W 2003 *Phys. Rev. Lett.* **90** 167401
[5] Yu L B, Lin D Z, Chen Y C, Chang Y C, Huang K T, Liaw J W, Yeh J T, Liu J M, Yeh C S and Lee C K 2005 *Phys. Rev.* B **71** 41405
[6] Moreno E, García-Vidal F J and Martín-Moreno L 2004 *Phys. Rev.* B **69**
[7] Raether H 1988 *Surface Plasmons on Smooth and Rough Surfaces and on Gratings* (Berlin: Springer-Verlag)
[8] Moreno E, Martín-Moreno L and García-Vidal F J 2006 *J. Opt. A: Pure Appl. Opt.* **8** S94
[9] Nikitin A Y, García-Vidal F J and Martín-Moreno L 2009 *Appl. Phys. Lett.* **94** 063119
[10] Zhang X and Li C 2009 *Physica* E **41** 1445
[11] Barnes W L, Dereux A and Ebbesen T W 2003 *Nature* **424** 824
[12] Stoyanov N S, Ward D W, Feurer T and Nelson K A 2002 *Nature Mater.* **1** 95
[13] Saxler J, Rivas J G, Janke C, Pellemans H P M, Bolivar P H and Kurz H 2004 *Phys. Rev.* B **69** 155427
[14] Seo M A, Park H R, Koo S M, Park D J, Kang J H, Suwal O K, Choi S S, Planken P C M, Park G S, Park N K, Park Q H and Kim D S 2009 *Nature Photonics* **3** 152
[15] Wang K and Mittleman D M 2004 *Nature* **432** 376
[16] Taflove A and Hagness S C 2000 *Computational Electrodynamics: The Finite-Difference Time-Domain Method* (Boston: Artech House)
[17] Lidorikis E, Povinelli M L, Johnson S G and Joannopoulos J D 2003 *Phys. Rev. Lett.* **91** 23902
[18] Ordal M A 1983 *Appl. Opt.* **22** 1099
[19] Kong J A 1975 *Theory of Electromagnetic Waves* (New York: Wiley-Interscience)
[20] Li Z Y, Gu B Y and Yang G Z 1998 *Phys. Rev. Lett.* **81** 2574